LEVEL
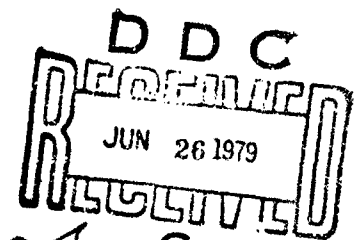
ADA070461

A Filled Silicone Rubber Materials System with Selectable Acoustic Properties for Molding and Coating Applications at Ultrasonic Frequencies

D D C

JUN 26 1979

C

May 11, 1979

DDC FILE COPY

REPORT DOCUMENTATION PAGE		READ INSTRUCTIONS BEFORE COMPLETING FORM
1. REPORT NUMBER NRL Report 8301	2. GOVT ACCESSION NO.	3. RECIPIENT'S CATALOG NUMBER
4. TITLE (and Subtitle) A FILLED SILICONE RUBBER MATERIALS SYSTEM WITH SELECTABLE ACOUSTIC PROPERTIES FOR MOLDING AND COATING APPLICATIONS AT ULTRASONIC FREQUENCIES		5. TYPE OF REPORT & PERIOD COVERED An interim report on a continuing NRL problem.
		6. PERFORMING ORG. REPORT NUMBER
7. AUTHOR(s) R. D. Corsaro and J. D. Klunder		8. CONTRACT OR GRANT NUMBER(s)
9. PERFORMING ORGANIZATION NAME AND ADDRESS Naval Research Laboratory Washington, D.C. 20375		10. PROGRAM ELEMENT, PROJECT, TASK AREA & WORK UNIT NUMBERS 81S01-46, RR011-08; 81S01-49B, SF43-452; 81S01-84, SF11-121
11. CONTROLLING OFFICE NAME AND ADDRESS Naval Research Laboratory Washington, D.C. 20375		12. REPORT DATE May 11, 1979
		13. NUMBER OF PAGES 35
14. MONITORING AGENCY NAME & ADDRESS(if different from Controlling Office)		15. SECURITY CLASS. (of this report) Unclassified
		15a. DECLASSIFICATION/DOWNGRADING SCHEDULE

16. DISTRIBUTION STATEMENT (of this Report)

Approved for public release; distribution unlimited

17. DISTRIBUTION STATEMENT (of the abstract entered in Block 20, if different from Report)

18. SUPPLEMENTARY NOTES

19. KEY WORDS (Continue on reverse side if necessary and identify by block number)

Anechoic Coating
Sound Absorbing Material Acoustic Properties
Ultrasonic Absorbers
Acoustic Material

20. ABSTRACT (Continue on reverse side if necessary and identify by block number)

This paper describes a convenient system of materials that can be used to prepare molded articles or spray-deposited thin coatings of materials with well-defined and continuously variable bulk acoustic properties. The system consists of four components. First, RTV-602 (with catalyst) is used as the rubber base; it is convenient to work with, has a low longitudinal absorption, and does not readily support shear waves. Second, typically one of four microballoon types is added, usually in the quantity necessary to obtain the desired attenuation coefficient. Third, an appropriate amount of ferric oxide is added to achieve the required impedance match, sound speed, or density.

(Continued)

DD FORM 1473 EDITION OF 1 NOV 65 IS OBSOLETE
1 JAN 73
S/N 0102-014-6601

20. ABSTRACT (Continued)

Finally, toluene is used to dilute the mix to a usable viscosity; we have found that toluene can be added in even large quantities and later removed, either before or after curing, without altering the final properties of the resulting rubber.

Equations are presented which allow the reliable prediction of longtiudinal wave speed, attenuation, impedance, and density over the useful range of composition variation. These equations were constructed using acoustical measurements at frequencies from 2.5 to 7 MHz, and from direct (immersion) density determinations. Echo-reduction measurements on flat plates have been used to verify that the spray deposition technique described here does not significantly alter the acoustical properties of these composite mixtures.

CONTENTS

A Filled Silicone Rubber Materials System with Selectable Acoustic Properties for Molding and Coating Applications at Ultrasonic Frequencies

INTRODUCTION

In our recent laboratory studies, we have had a recurring need for molded articles and thin (anechoic) coatings, constructed of materials with well-known and user-selected acoustic properties. The bulk acoustic properties of particular interest are sound speed, sound absorption, and density (for acoustic impedance). The required values of these parameters span a wide range.

Examples of our studies with such needs include testing theoretical descriptions for sound interaction with coated and uncoated geometrical shapes (spheres, cylinders, scale models of naval platforms and submersibles -- see, for example, [1,2 and 3]) and optimization of acoustic devices through material selection (waveguided parametric arrays, random rough surface coatings [4,5]).

Initially the needs of these various studies could be met largely by hit-or-miss material selection. More recently, however, the acoustical requirements became too restrictive to be satisfied in this manner. Hence, we initiated this present attempt to develop a system of materials that could be used to fill our needs.

For our purposes, filled-rubber composites are most applicable. The components needed include a rubber base, and one or more inert fillers; these fillers are used to modify the acoustic properties of the final composite. By careful selection of filler type and concentration, we can prepare rubbers offering a wide choice of acoustic properties. For example, by selecting either a high or low density filler, rubber composites can be made offering a wide range of density variability.

Selection of an appropriate rubber base is of great importance. An initial requirement is that it be relatively easy to work with in the laboratory, and its curing procedure be consistent with small-batch laboratory applications. While this requirement is not difficult to meet, it is nonetheless important to mention, since some of the articles to be coated are quite fragile and will not withstand even moderately elevated (or depressed) temperatures or pressures. Additionally, a diluent must be available for the rubber base chosen, since the addition of even low concentrations of filler rapidly increases the viscosity of these mixes to the point where they will not completely fill the mold used. The use of diluents generally complicates the data analysis, since the presence of an additional material component must be included, but this is a complication that can be handled under usual circumstances.

A major difficulty in this selection, however, is imposed by the requirement that these materials be deposited as thin coatings by using a spraying technique; that is, by spraying through commercial-type paint sprayers. To obtain the very low viscosities this requires, a considerable amount of diluent must be used in the mix. However, for curing, this diluent must be removed after spraying. Assuming that such a diluent can be found, it is further necessary that the temporary presence of diluent in the mix will not significantly affect the acoustic properties of the final rubber.

This report details the major tasks in the order in which they were attempted. First, the system of materials that we have determined to be ideal for our purposes is described. Next, the experimental procedures used in the evaluation of the acoustic properties are explained. The two following sections present the data reduction procedure, and the fitting equations. An analysis of the sound speed and density data, based on the ideal mixture model and a discussion of the fitting equation used for the absorption data follows. Finally, there is a test of coating predictability; echo reduction measurements of coated flat plates are compared with theoretical predictions, based on the predicted bulk acoustic properties. This comparison allows us to determine if the applied coatings have the same material properties as the bulk mix from which they were formed.

MATERIALS USED

The system of materials used consists of a rubber base, diluent, and high and low impedance fillers.

Rubber Base (abbreviated R602): The rubber or resin base used is type RTV-602 from General Electric Corporation. This silicone rubber was chosen for a number of reasons: it is readily available, easy to use (having a room temperature cure), and has a low sound absorption. Particularly important to this application, R602 is cured by the addition of a small amount of catalyst (type SRC-05), which suggests that its chemical structure (and the kinetics of curing) is amenable to dilution.

Diluent (toluene): a diluent is required to reduce the viscosity of these mixes, both for preparing molded articles and spraying thin coatings (using a pressurized-feed paint sprayer). The latter application (spraying) imposes a considerable constraint on the diluent; it must be possible to add sufficient diluent to achieve a water-like consistency. Of approximately eight potential diluents tested, only toluene was found to be satisfactory.

Our data suggest that this diluent is ideal; it can be easily driven off, either before or after curing, without noticeably influencing the properties of the cured rubber. This was demonstrated by making up three poured samples, one without toluene, and two with appreciable amounts of toluene added. All three were poured into molds, and then one of the samples with added toluene was placed under vacuum until the odor of toluene could no longer be detected. All three samples were allowed to cure, and stand for one week, to allow time for the toluene in the remaining sample to evaporate (judged by odor). Density, sound speed, and sound absorption measurements were then made. In all cases, the measured values were independent of which sample was used. This procedure was carried out three times: once using only the pure rubber, and twice more with SGMB and FFOX additives (filler types to be described later). The results were the same in all three cases.

The important result of these tests is that the temporary presence of toluene in these samples apparently does not influence the acoustic properties of the resulting filled rubber; the toluene initially added can therefore be ignored in all of our calculations.

Heavy Fillers: For essentially all samples prepared, reagent grade ferric oxide (FEOX) was used as the dense filler (obtained from Fisher Scientific Co.). This filler was chosen because it is denser than water (5.04 g/cc), is readily available, and easy to work with. It is also familiar — "rust".

Initially, finely powdered lead was used. The usual advantage of lead in these applications is that, because of its high density, only a small volume fraction need be used to significantly increase the density of the mix. In our present application, however, the very high density of lead became a disadvantage; in the very low viscosity mixes, lead powder tends to settle to the bottom of the container. Hence, we select a somewhat less dense filler for these applications. It is also noted that, by using ferric oxide, we eliminate the toxicity hazard associated with using a finely divided lead powder.

Light Fillers: data were collected on four readily-available low-density fillers. All are microballoons (hollow spherical shells, filled with air or nitrogen) less than 0.1mm in diameter. Additional properties of these microballoons are presented in Tables 1 and 2.

Table 1 — Ideal Mixture Parameters — Experimental

Code	Name	Density (TPD)* (g/cc)	Sound Speed (TPSS)* (m/s)
R602	RTV-602 silicone resin	1.007	1018
FEOX	Iron oxide	5.04	5000
SGMB	Small glass microballoon	0.242	3500
LGMB	Large glass microballoon	0.332	3300
BKMB	Bakelite microballoon	0.379	1900
TBMB	Thin-wall Bakelite microballoon	0.232	1300

*TPD is a true particle density, and TPSS is the corresponding sound speed calculated in a similar manner.

---SGMB (small glass microballoons) type FTF-15 from Emerson and Cuming Inc., composed of a high-silica insoluble glass (softening point, T_s, is 1093° C).

---LGMB (large glass microballoons) type IGD-101, also from Emerson and Cuming Inc., composed of sodium borosilicate glass (T_s = 482°C).

---BKMB (Bakelite microballoons) type BJO-0840, from Union Carbide Corporation, composed of Bakelite acrylic resin. This is a relatively high density (thick wall) Bakelite microballoon.

---TBMB (thin-wall Bakelite microballoons) a lower density balloon, type BJO-0931, from the same source.

Table 2 — Ideal Mixture Parameters — Theory

Property	SGMB	LGMB	BKMB	TBMB
SIZES				
True particle density (g/cc)	0.242	0.332	0.379	0.232
from manufacturer	0.33	0.30	0.25-.35	0.15-.20
Diameter (μm) (approximate ave.)	20	60	43	43
Wall thickness—from density (μm)	0.36	1.6	2.6	0.84
SHELL MATERIAL PROPERTIES				
Similar material type	Pyrex	Crown	Lucite	Lucite
Density of shell (g/cc)	2.31	2.23	1.18	1.18
Bulk Modulus ($\times 10^{-10} N/m^2$)	3.97	3.40	0.67	0.67
Shear Modulus ($\times 10^{-10} N/m^2$)	2.5	1.81	0.143	0.143
Sound Speed — Longitudinal (m/s)	5640	5100	2680	2680
— Compressional (m/s)	4150	3905	2382	2382
ASSEMBLAGE				
K^* ($\times 10^{-10} N/m^2$)	0.2018	0.2304	0.0635	0.0199
Sound Speed (m/s)	2890	2650	1295	1178

Figure 1 is a microphotograph of a typical composite. Two scales are superimposed over the object: the upper ruling corresponds to 25 μm (1 mil) increments, and the lower ruling is in increments of 10μm. The rubber composite shown contains two fillers: FEOX particles, which are not distinguishable at this degree of magnification, but which impart a red coloration to the entire sample, and SGMB which are visible as spherical microballoons, approximately 20 μm (0.8 mil) in diameter.

EXPERIMENTAL PROCEDURES

The experimental procedures used to evaluate the acoustic properties are, for the most part, routine. Hence, they are only briefly discussed here.

Density is determined by the usual technique of liquid displacement. Each sample (approximately 25 cc volume) is weighed first in air, and then again when totally submerged in water. From these two weights (w and w' respectively), and the known (temperature corrected) density of water, D_w, the density of the sample, D, is calculated, using the equation:

$$D = D_w/w(w - w') \qquad (1)$$

The major potential error associated with the use of this technique lies in the possible presence of air bubbles, which attach themselves to the surface of the sample. To reduce this error, the container of water, with the sample submerged, is placed under vacuum for one minute prior to weighing; during this evacuation, the container is tapped repeatedly to dislodge

4

Fig. 1 — Microphotograph of coating material. Spherical cavities shown are glass microballoons (SGMB).

the larger bubbles. Although some small bubbles remain, they do not affect the density determination to within the level of precision that is required here.

Acoustical measurements (sound speed, absorption, and echo reduction) are all made using the small tank shown in Fig. 2. This tank has inside dimensions of 10 × 15 × 30 cm. A transducer is firmly attached to either end, allowing 20-cm separation between their front faces. The samples were placed near the midpoint of the tank, in a holder which allows 2-axis angular adjustment, to obtain normal incidence of the sound beam. For sound speed and absorption measurements, the samples used have a cross section of 9 × 9 cm, and a thickness of 0.15 to 2.0 cm. The sample used in each case is the thickest that still presents a usable acoustic signal to the receiving transducer. For the echo reduction measurements, the coatings were fabricated on thick steel plates measuring approximately 10 × 17 cm in cross section, and 1.9 cm thick. The surface of these plates was ground flat (32 finish or better) prior to the coating application.

Figure 3 is a block diagram of the electronics. This arrangement is used, via switches or cable exchanges, to perform the three separate acoustical measurements required.
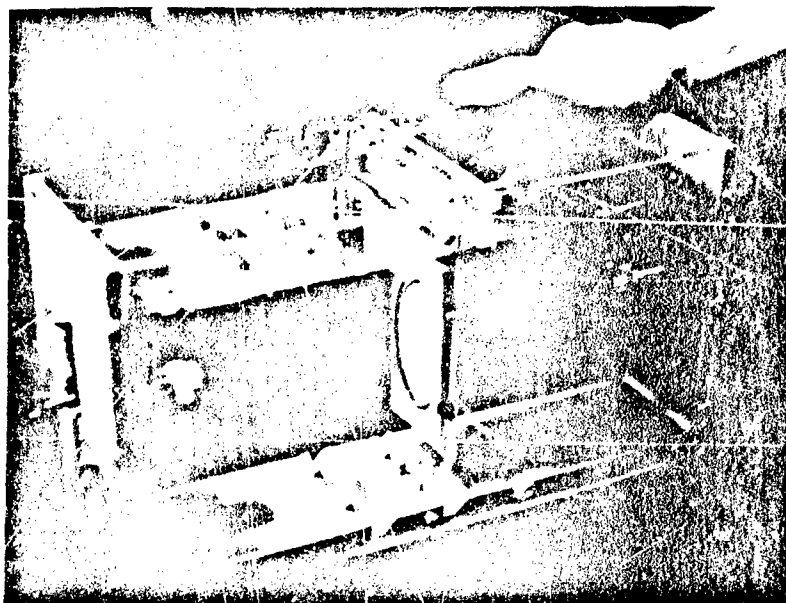
Fig. 2 — Photograph of the tank used for the ultrasonic measurements. Configuration shown
is as used in absorption measurements: sample is mounted in the middle of the tank.

For sound speed measurements, the transmitting transducer is driven by a single (repeti-
tive) short-duration pulse, of approximately 50 V amplitude, as obtained from the pulse genera-
tor. The signal received by the other transducer consists of only a few cycles of sound, and is
displayed on the oscilloscope.

Sound speed is then determined by measuring the change in travel time upon insertion or
removal of the sample. Actual travel time is defined as the time required for the sound pulse
to travel from the transmitter to the receiver; it does not have to be measured directly since we
only require the change in travel time caused by the presence of the sample. This change is
visually measured on the face of the oscilloscope. Obviously, if there is no change in signal po-
sition upon insertion of the sample, the speed of sound in the sample, C_x, must be the same as
that in the water displaced, C_w. More generally sound speed is determined from the change in
travel time, t, using the relationship:

$$1/C_x = (t/d) + (1/C_w) \qquad (2)$$

where d is the sample thickness.

This technique is well suited for measuring sound speed in these (usually) highly absorb-
ing samples. It only requires a detectable received signal, obtained by one direct pass through
the specimen. The principal source of error associated with its use is wave distortion, caused by
velocity dispersion in these highly absorbing materials. To minimize these errors, we ignored
the sinusoidal nature of the received signal (which is related only to phase velocity), and in-
stead made all time-interval measurements from the leading edge of each signal: the first occu-
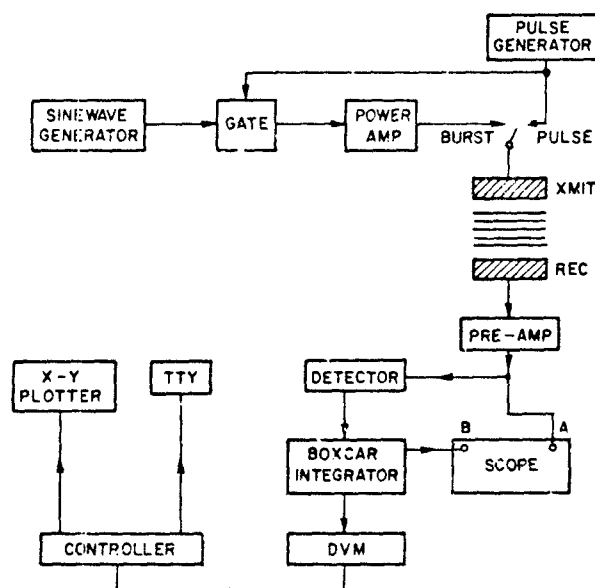rance of a deviation from the base line which is 5% of the maximum positive amplitude of the

6

Fig. 3 — Block diagram of the electronics used

received wave packet. Sound speeds obtained in this manner should essentially correspond to group velocities, although it is recognized that the selection of this criterion is subjective and operator dependent.

Sound absorption is measured using essentially the same apparatus, however in this case the transmitter is driven to form a sound burst. This sound burst is obtained by gating the continuous sinusoidal output of a frequency generator, to pass (repetitively) wave packets containing ten or more cycles. For highly absorbing samples, the duration of each burst is limited only by consideration of the internal reflections within the tank, since reflections within the sample will be greatly attenuated. For samples with low sound absorbtion, where internal reflections within the sample could be of appreciable magnitude, their influence is avoided by using only thick samples and short burst durations, and making all amplitude measurements on the first echo in the received echo train.

The sound absorption coefficient α is then calculated from the measured values of received sound pressure level, both with (P_i) and without (P_o) the sample in the tank. The equation used is:

$$\alpha \ (\text{dB/cm}) = (20/d) \log \{P_o/[P_i (1 - R^2)]\} \tag{3}$$

The reflection coefficient R must be included since a portion of the detected signal reduction is due simply to reflection losses at the two surfaces of the sample. The value of R was estimated from the usual equation for simple reflection, namely $R = (Z_1 - Z_2)/(Z_1 + Z_2)$, where Z_1 and Z_2 are the simple acoustic impedances (density times sound speed) of the two media.

We have determined that the imaginary portion of the reflection coefficient can be neglected in this calculation of absorption for the particular experimental procedure used. This was established by including the imaginary portion of R in Eq. 3, using the previously calculated value of absorption in a successive approximation technique. In all cases tested the final calculated value of absorption was only slightly influenced. This is reasonable, since the samples measured were always more than a few wavelengths thick. Thus, for highly attenuating media the reflection loss is small compared with the overall signal attenuation, and for low absorption media the imaginary part of R is negligable compared to the real part.

Echo reduction is measured as the ratio P_x/P_r, where P_x is the echo amplitude returned from the sample, and P_r is that from an uncoated (reference) steel plate. Since steel is only 95% reflective, the values thus obtained are then increased by 0.5 dB, to normalize them to an ideally rigid reference. The equation used is:

$$ER = -20 \log (P_r/P_x) + 0.5 \qquad (4)$$

The acoustic signal was again a sound burst, where the duration of the burst was sufficiently short not to include reflections within the steel plate. The signal amplitude ratio measured, P_x/P_r, is identically that for the coating placed on an infinitely thick steel plate. Since these coatings are quite thin, much thinner than the steel plate, essentially all echoes within each coating are included (summed) in the received echo. Hence, the echo reduction calculated using Eq. 4 corresponds to what one would obtain using a continuous signal, for a coating applied to an infinitely thick, rigid backing.

Because of the large number of data points required to adequately represent the frequency dependence of echo reduction, an automated data acquisition system was assembled. Using this system, echo reduction was measured over the frequency range shown in the figures, in frequency increments of 0.1 MHz. As shown in Fig. 2, the amplitude of the received signal is converted to a DC voltage using the boxcar integrator (with a detector on the front end, and the sampling gate positioned over the echo of interest). This DC voltage is then digitized, and linearized (using an internally stored calibration table) by the HP 9100A programmable calculator. In use, one first collects data with an uncoated steel plate in the tank, and stores the resulting reference signal amplitudes in a second table within the calculator's memory. This reference data is collected over the entire usable frequency range of the transducers used. Then a coated plate is placed in the tank, and the data collected in this case is divided by the reference level, converted to decibels, and plotted on an X-Y plotter. Once a run is begun, the only operator involvement is to change plates, and change frequencies on command from the controller. Although frequency changing could easily be performed by the controller, rather than by the operator, an interfacial frequency source was not available.

8

SOUND SPEED, DENSITY, AND IMPEDANCE

The sound speed and density data collected are found to be in good agreement with the predictions of the ideal mixture model (also called the simple rule of mixtures). Therefore, we find it convenient to first present the behavior predicted by this model, and then show its agreement with the data.

Ideal Mixture Predictions

As shown in Appendix B, the ideal mixture model assumes only that there is no volume change upon mixing the components of a mix. From this one simple assumption, equations for density ρ and compressibility κ are found:

$$1/\rho = \sum (V_i/\rho_i) \tag{5}$$

$$\kappa = \sum (V_i \kappa_i) \tag{6}$$

where V_i represents the volume fraction of each component, ρ_i and κ_i are respectively the densities and compressibilities of the pure components, and the sum is taken over all components. The longitudinal sound speed C and acoustic impedance Z can then be calculated using the usual equations:

$$C = 1/\sqrt{\rho \kappa} \tag{7}$$

$$Z = \rho C \tag{8}$$

Rather than using the compressibilities of the pure components as parameters, it is conceptually easier to use the equivalent compressional wave speeds (neglecting shear) for the pure components, as defined by Eq. 7. Hence, we need not refer to compressibilities here, although it is recognized that they are calculated as intermediate steps.

The pure component parameters used in these model predictions are given in Table 1. These were actually determined (in most cases) by fitting the data collected to obtain best values. For the present discussion, however, we will ignore the origin of these parameter values, and return to their origin somewhat later in this section.

Figure 4 shows the calculated dependence (lines) of density for mixtures containing R602 with two fillers: FEOX and SGMB. Here, density is graphed against the weight fraction of resin (R602) in the mix; the addition of either filler (FEOX or SGMB) will proportionately decrease the amount of resin. Starting with the pure resin (weight fraction = 1), the addition of dense filler (FEOX) is seen to increase the density of the mix (uppermost curve), and correspondingly the addition of the less dense filler (SGMB) is seen to decrease its density (lowermost curve). The other lines drawn are for multi-filler mixes, that is, mixtures simultaneously containing both FEOX and SGMB. Along any line the weight fraction of the appropriate filler can be found by tracing back to its intersection with one of the two single-filler curves. All lines are extended to include only those compositions containing greater than 40% resin phase by volume; if less resin is present, packing of the fillers can play an important role.

In a similar manner, Fig. 5 shows the predicted behavior of sound speed in these same mixes (lines). The addition of FEOX to pure resin is seen to decrease the sound speed over
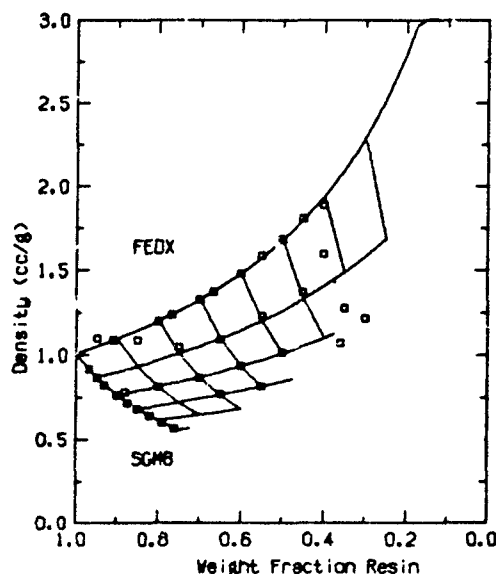
Fig. 4 — Density of mixes containing SGMB

most of the usable range of compositions, while the addition of SGMB greatly increases it. Figure 6 shows the predicted impedances of these mixes. As might be expected, the addition of dense filler, FEOX, increases the impedance, while the addition of the less dense filler, SGMB, decreases it.

Figures 7, 8, and 9 show similar graphs for BKMB. Although the magnitudes of the changes are somewhat different from those of SGMB, the general behavior is seen to be similar. Figures 10 ,11 and 12 show the predictions for the addition of LGMB, and Figs. 13, 14 and 15 correspond to the addition of TBMB.

Data Collected

The data collected in this study are shown as squares in Figs. 4 thru 12. It is now clear why the theoretical predictions were presented first; without the backgound coordinate lines drawn from theory, it is awkward to distinguish the composition of the mix corresponding to each data point.

It will now be shown that the agreement between theory and experiment is good. Consider again Fig. 4. The data points along the uppermost curve are for samples containing only FEOX as the filler; the data points along the lowermost curve similarly are for samples containing only SGMB as the filler. In both cases the data points are well described by the lines drawn, which represent ideal-mixture predictions. For mixes containing both fillers simultaneously, the compositions used experimentally correspond to the points of intersection of the theoretically predicted curves. From the observation that the data points appear very close to these intersections, we again conclude that the agreement between theory and experiment is quite good, even for these three component mixes (R602, FEOX, SGMB) with rather high concentrations of fillers.
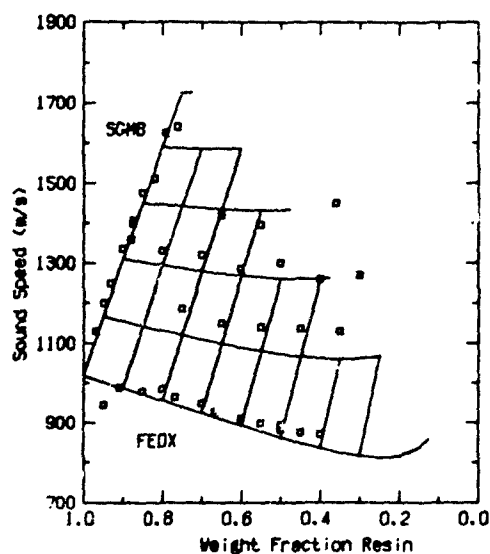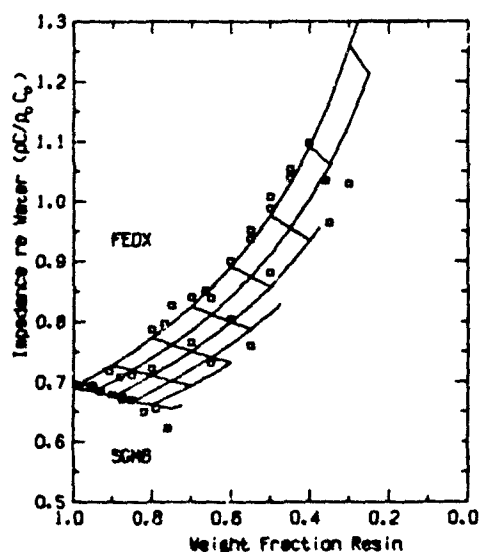
Fig. 5 — Sound speed in mixes containing SGMB

Fig. 6 — Simple impedance (relative to water) of mixes containing SGMB

Figure 5 is a simular graph, but in this case for sound speed data. The agreement between data (squares) and theory (lines) is again seen to be good, although not quite as good as was the case for density. The small disagreement between theory and experiment in this case is due primarily to the high uncertainty associated with the measurement of sound speed in these highly absorbing media. Considering this error source, the agreement is quite acceptable. Two additional potential sources of error should also be mentioned. First, in the case of sound speed, the reliability of ideal mixture theory is somewhat reduced, since sound speed is related to the volume derivative, it is somewhat more sensitive to devir ions from this theory. This potential error source is presumed, at this time, to be only a minor contributor. Second, we recall that the shear term has been neglected in these sound speed evaluations. For this rubber, with low concentrations of fillers, this neglect is justifiable. On the other hand, the neglect of shear is probably not justifiable for samples containing appreciable amounts of microballoon fillers (judging from the inflexibility of these samples). Nevertheless, since we are not presently prepared to measure shear modulus, we will continue to neglect this term.

Figure 6 shows the behavior of impedance, where each data point graphed here is simply the product of the density and sound speed data shown in the two preceeding figures. As such, the error limits associated with each data point are quite large. This figure is included for two reasons. First, it is very useful in assigning fitting parameters, since it is more sensitive to small deviations than either the sound speed or density graphs. Second, this figure displays the range of variability of impedance which can be achieved with each mix, and the approximate compositions which are useful for impedance matching
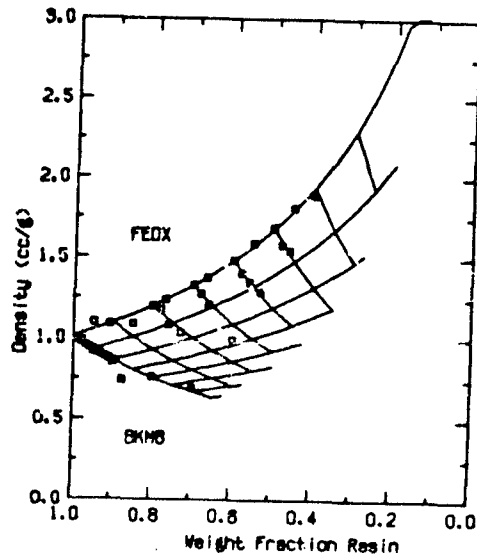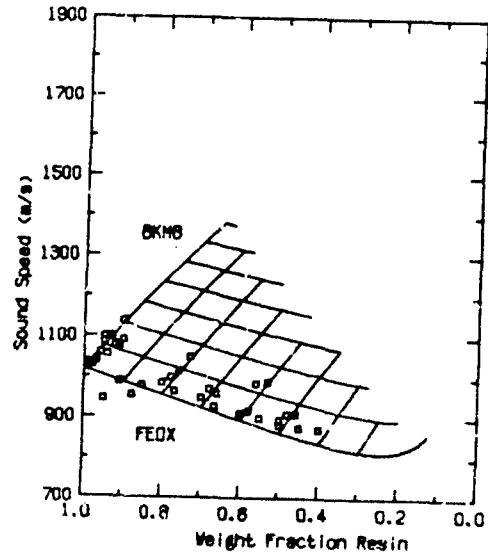
Fig. 7 — Density of mixes containing BKMB
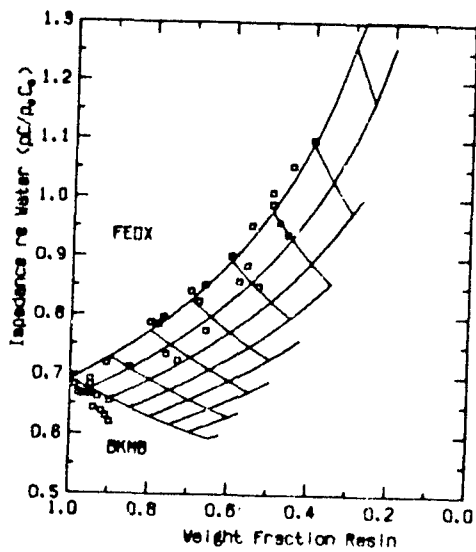

Fig. 8 — Sound speed in mixes containing BKMB

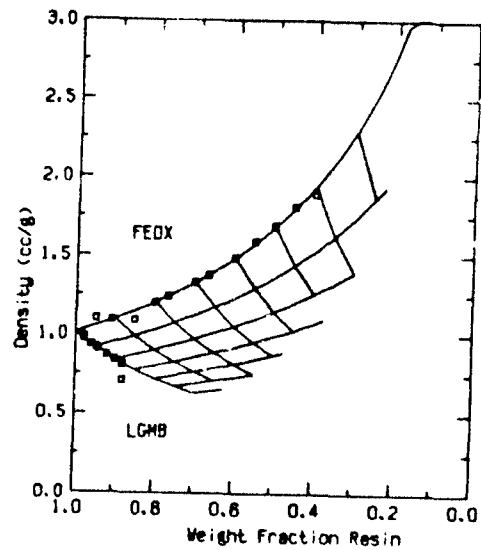Fig. 9 — Simple impedance (relative to water) of
mixes containing BKMB

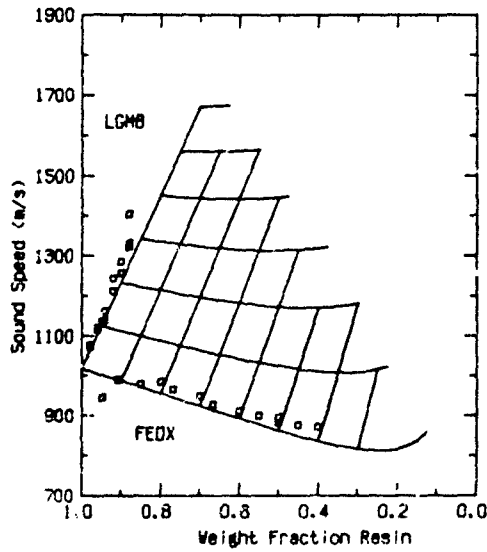Fig. 10 — Density of mixes containing LGMB
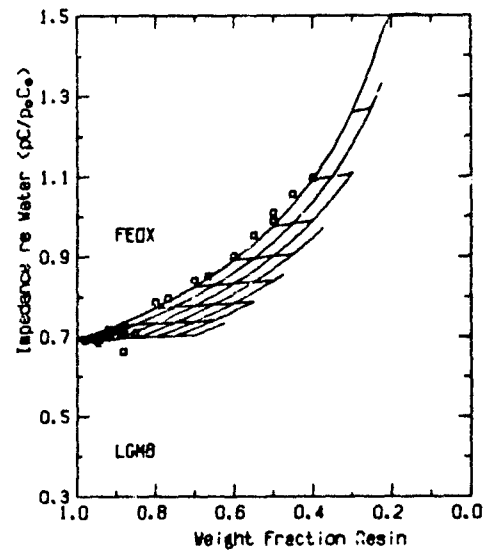
Fig. 11 — Sound speed in mixes containing LGMB

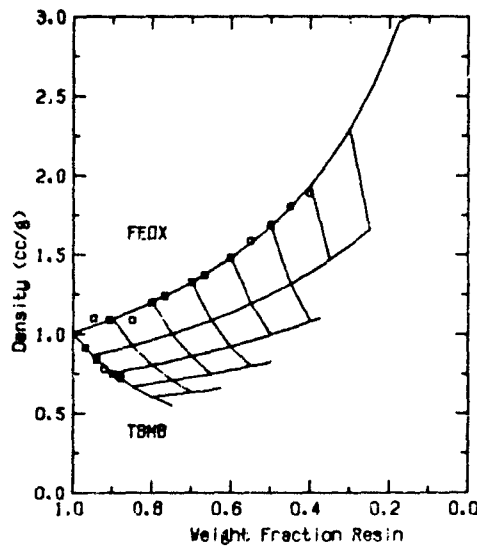Fig. 12 — Simple impedance (relative to water) of mixes containing LGMB

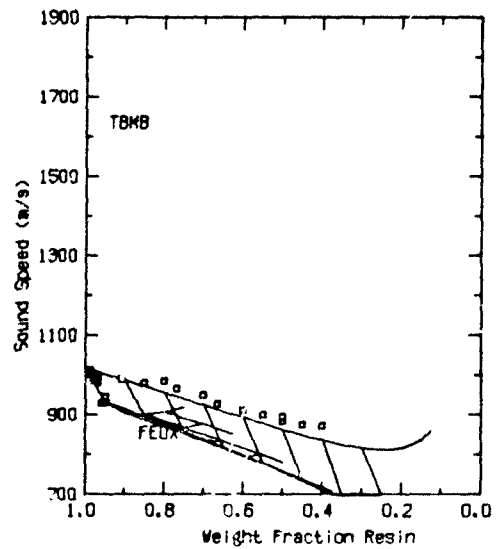
Fig. 13 — Density of mixes containing TBMB

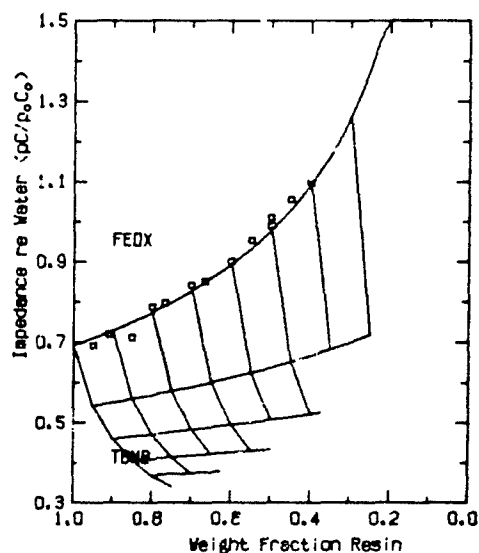Fig. 14 — Sound speed in mixes containing TBMB

13

Fig 15 — Simple impedance (relative to water) of
mixer containing TBMB

Simular data are shown in Figs. 7, 8, and 9 for the case of BKMB, but with one important distinction; the compositions tested (0.02, 0.04, and 0.07 weight fraction BKMB) do not match the compositions used in the theory calculations, and so, some interpolation is nesessary to judge the agreement between theory and experiment. Our conclusion is that the agreement is again highly satisfactory.

The remaining figures of this series (Figs. 10 through 15) include little experimental data — just enough for parameter determinations. In view of the good agreement obtained between theory and experiment in the other two cases (SGMB and BKMB), we decided that the collection of additional data of this type is not necessary.

Fitting Parameters Used

The pure-component densities and sound speeds listed in Table 1 are determined by use of a best fit to the data collected. Some of these parameters, however, can be independently estimated. In particular, the values listed in Table 1 for the pure resin (R602) were actually evaluated from direct measurements on the pure material. These are in excellent agreement with those reported by Ryder [4] (density — 1.009 g/cc, sound speed — 1018 m/s). Further, the density of FEOX is in agreement with that reported [6] for the crystalline material (iron (III) oxide: density — 5.24 g/cc), while the sound speed tabulated is consistent with that of similar dense and incompressible solids. This particular sound speed value does not require accurate evaluation, since the behavior predicted by ideal mixture theory is not particularly sensitive to small variations in this value.

Independent evaluations for the four microballoon types are less useful. This is because the detailed distributions of size and wall thickness are not known, and due to batch variability,

are not worth determining. Nonetheless, some rough estimates are obtainable, and can be of practical use in the preliminary selection of filler type. The values of true-particle-density that appear in the manufacturers literature are given in Table 2, in parentheses. They are seen to be somewhat different from those values obtained in this study (values not in parentheses, from Table 1), even though the evaluation technique used in both cases is the same— liquid (or rubber) displacement. It is our conclusion, therefore, that the densities reported by the manufacturers can serve as only a rough guide for choosing between microballoons of different types.

Sound speed estimates for these microballoon fillers is even more precarious. There are several equations available for predicting the equivalent bulk modulus of the composite K^*, knowing only the composite density ρ_c, and properties of the shell material such as its density ρ, bulk modulus K, and shear modulus S. It is generally conceded, however, that all such equations are presently unreliable. For example, the well known composite - sphere - assemblage model [6], as applied to this case of (essentially) evacuated microballoons, finds $K^* = 4KS(1-b)/(4S+3Kb)$, where b is $1+(\rho_c/\rho)$ Using this equation, we can predict the effective bulk modulus of the composite, and estimate wave speed from the following equation:

$$C = \sqrt{K^*/e} \qquad (9)$$

As shown in Table 2, sound speed values calculated in this manner all fall somewhat lower than those determined experimentally. Interestingly, Haskin [7] notes that these predictions should represent upper limits, where the corresponding lower limit in all cases is approximately the speed of sound in air. The cause of these disagreements between experiment and theory are probably due to two deficiencies: the limitations of these idealized theories, as discussed by Haskin, and the use of experimental data which was obtained by an extrapolation from only dilute solution measurements.

ABSORPTION

Approach Used

In fitting the absorption data collected, some use is made of functional dependences that are theoretically predicted. Principally, the results presented by Allegra and Hawley [8] are utilized. In most cases, however, our experimental data does not support the rigorous application of these theortical results. While this is unfortunate, it is also not particularly important. For our present application we require only a phenomenological fitting equation which describes the absorption data collected, and any theortical justification is irrelevent. We include mention of the available theory only because it guided our development of the fitting equation, but we do not hesitate to modify the functional form of the fitting equation if a better data fit can be obtained.

The theoretical treatment of Allegra and Hawley indicates that for dilute suspension the absorption due to the addition of the suspended material is of the form:

$$\alpha = A \; V \; f(F) \qquad (10)$$

where A is a proportionality constant, V is the volume fraction of suspension, and $f(F)$ is some function of frequency. In the limiting case of suspended particle which are small compared to the wavelength of sound used, $f(F)$ is the square of frequency, while for the limiting

case of particles which are much larger than the wavelength, $f(F)$ is the square root of frequency.

The materials studied here bear some resemblance to the case analyzed by Allegra and Hawley, however there are some significant differences also. Principally, the concentration of filler used (suspended medium) is not small, but can be quite large. This introduces cooperative absorptive losses, such as multiple scattering terms. Further, most of the compositions of practical interest here involve the simultaneous use of two or more fillers, both of which may be present in large concentrations. Without belaboring the point, it is clear that the treatment of Allegra and Hawley cannot be rigorously applied; we can, however, attempt to retain the general form and separation of variables evident in Eq. 10.

The starting point in our analysis is to describe the absorption due to the addition of each filler to the rubber base, without the presence of any other fillers. For each filler, indicated by the subscript i, we then analyze the absorption data collected using the following equation

$$\alpha_i = A_i f(V) f(F) \tag{11}$$

where A_i is the proportionality constant, $f(V)$ is a function of the volume fraction of filler i, and $f(F)$ is a function of frequency. This separation of volume and frequency dependences is consistent with the formulation of Eq. 10, and is convenient both, in reducing the experimental data, and in using the fitting equations developed for predictive and materials-selection applications.

After developing fitting equations for the separate addition of each of the fillers to the rubber base, we can then consider the simultaneous addition of two fillers.

Fitting Equations Used

RTV602 — Although the sound absorption coefficient for the base rubber alone is quite small, it cannot be ignored. As shown in Fig. 16, the absorption data we collected appears to be linearly related to the square of frequency, but with a finite intercept at $F = 0$. The existance of this intercept is bothersome, and is probably due to the existance of a low-frequency relaxational process. To complicate matters, some tentative absorption data collected at 0.5 to 0.8 MHz consistantly falls below this intercept value, indicating that the presumed relaxation process has relaxational frequency components in the region 0.5 to 1.0 MHz. For this reason we have adjusted the functional form of the frequency dependence, to include the small low-frequency relaxational contribution, recognizing that the functional form used is highly spectulative but consistent with our data over the frequency range of interest in this study. The frequency dependence thus used is $F^2[1 + 3/(.5 + F^2)]$. For mixes containing fillers, we also assume that this absorption component will be proportional to the volume fraction of rubber base present. The final equation used is given in Table 3, where it is noted that the absorption due to this component of the mix is generally unimportant.

FEOX — Figure 17 shows the absorption data collected for mixtures containing only FEOX. In this figure, absorption is normalized by the volume fraction of FEOX, and is graphed versus frequency. Each symbol type indicates a different filler concentration; in Figs. 17 to 24, the most dilute mixes are represented by squares, and progressivly more concentrated mixtures are shown using circles, triangles, plus signs, crosses, diamonds, etc. The actual filler concentrations used are not documented here, but along with the raw absorption data, are available on request.
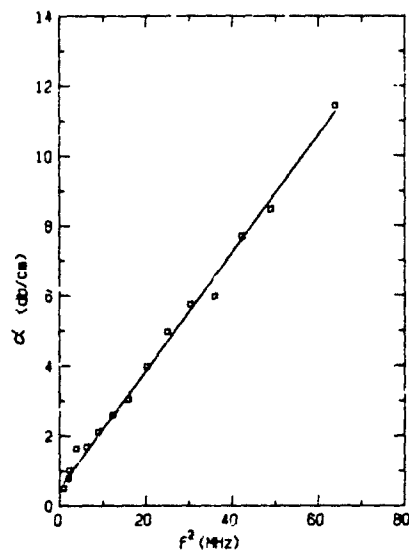
Fig. 16 — Frequency dependence of absorption for RTV-602. Line drawn is from the parameters of Table 3.

Table 3 — Absorption for Composites

$$\alpha(dB/cm) = \Sigma\ [A\ f(V)\ f(F)]$$

Component	A	$f(V)$	$f(F)$	$\alpha(dB/cm)$*
COMPOSITES CONTAINING ONE FILLER				
RTV602	0.168	V_r	$F^2(1+3/(.5+F^2))$	2.9
FEOX	196.	$V_f(.4-V_f)$	$F^{1.2}$	31
SGMG	11.3	$V_s(1.3-V_s)$	$F^2(1+8.2/(2+F^2))$	32
LGMB	48.8	$V_l(.67-V_l)$	$F^{2.2}$	59
BKMB	810.	V_b	$F^{0.55}$	170
TBMB	2630.	V_t	$F^2/(2.5+F^2)$	230
COMPOSITES CONTAINING FEOX AND FILLER LISTED				
SGMB	80.	$V_s\ V_f$	F^2	6.9
BKMB	1200	$V_b\ V_f$	$F^{0.5}$	24

*Calculated sound absorption at 4MHz for samples containing 10% by volume of (each) filler in a 90% RTV602 matrix.

By modifying the volume-fraction term, we can obtain better consistency between data collected for samples with differing filler concentrations. Figure 18 shows that the volume term
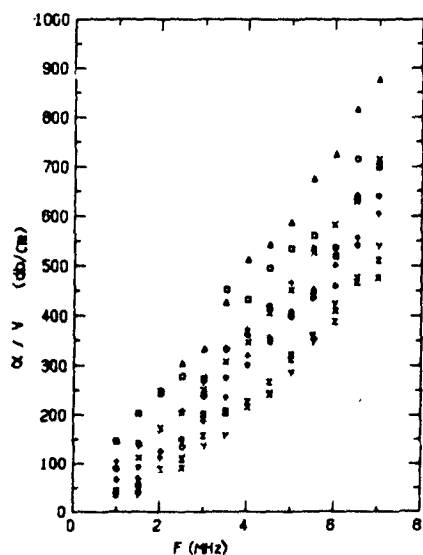
Fig. 17 — Frequency dependence of absorption, normalized by volume fraction, for FEOX.
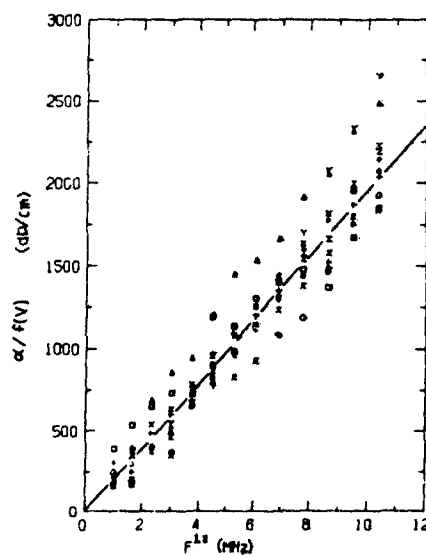

Fig. 18 — Data fit for absorption due to the addition of FEOX. Volume fraction is adjusted by: $f(V) = V_f(0.4 - V_f)$. Line is drawn using parameters of Table 3.
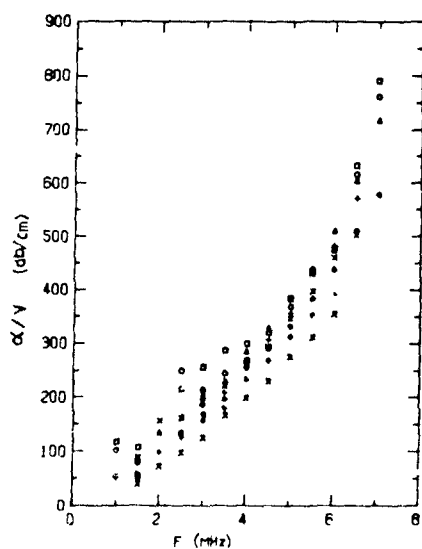

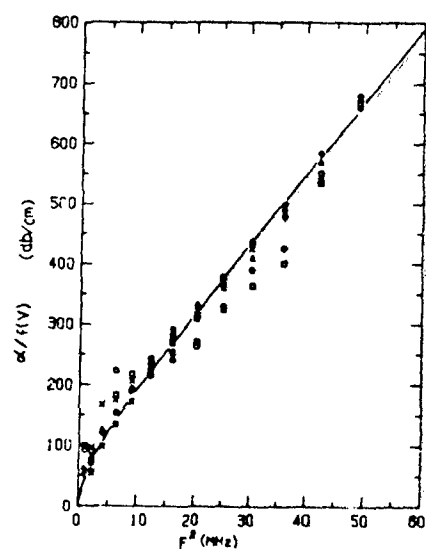Fig. 19 — Frequency dependence of absorption, normalized by volume fraction, for SGMB.

Fig. 20 — Data fit for absorption due to the addition of SGMB. Volume fraction is adjusted by: $f(V) = V_s(1.3 - V_s)$. Line is drawn using parameters of Table 3.

18

Fig. 21 — Frequency dependence of absorption, normalized by volume fraction, for LGMB.

Fig. 22 — Data fit for absorption due to the addition of LGMB. Volume fraction is adjusted by: $f(V) = V(.67-V)$. Line is drawn using parameters of Table 3.

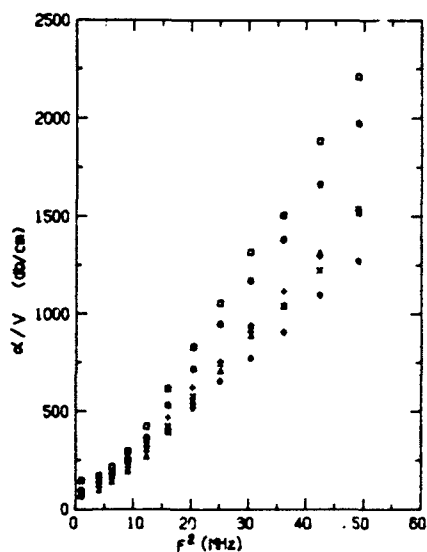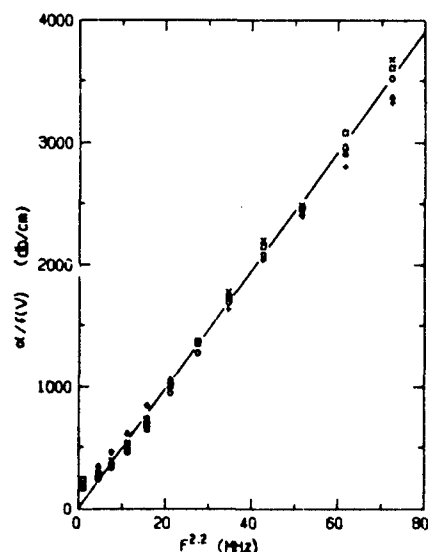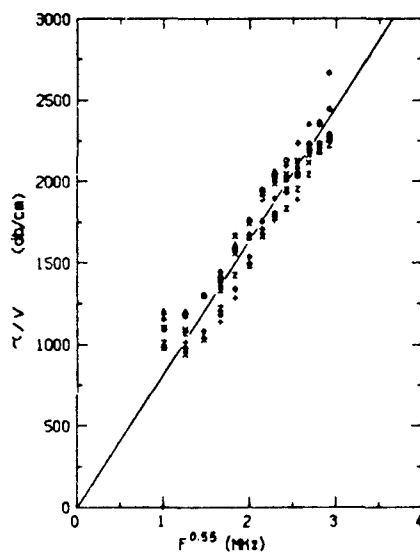Fig. 23 — Frequency dependence of absorption, normalized by volume fraction, for BKMB. Line is drawn using parameters of Table 3.
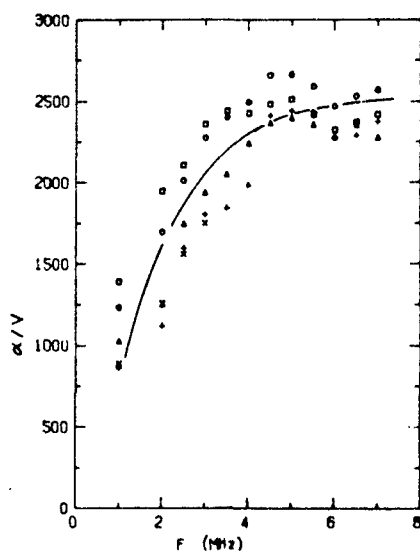
Fig. 24 — Frequency dependence of absorption, normalized by volume fraction, for TBMB. Line is drawn using parameters of Table 3.

19

$V_f(.4-V_f)$ gives an improved graph, and one in which the reduced absorption data is propor-tional to frequency raised to the power 1.2. The straight line drawn through the data symbols provides a useful representation of the absorption data collected, and the equation describing this line is given in Table 3.

SGMB — The absorption data collected for mixes containing only SGMB is shown in Fig. 19. Again, some adjustment is needed to the functional dependence of volume-fraction to ob-tain better consistency. Figure 20 shows that the volume-fraction dependence $Vs(1.3-Vs)$ is satisfactory for this purpose. The reduced absorption data is then seen to be approximately pro-portional to the square of frequency at the higher frequencies shown, however at frequencies less than 3 MHz a more gradual frequency dependence is required. The line drawn through these symbols corresponds to the frequency dependence $F^2[1 + 8.2/(2+F^2)]$, and it is seen to provide an adaquate representation of this data. The equation used to generate this line is given in Table 3.

LGMB — Figure 21 similarly shows the dependence of absorption on frequency squared for LGMB mixes. Once again, better consistency can be obtained by adjusting the volume-fraction term. Figure 22 shows that a suitable volume-fraction dependence is $V_l(.67 - V_l)$. Further, the reduced absorption data appears proportional to frequency raised to the power 2.2. The line drawn through the symbols corresponds to the equation presented in Table 3.

BKMB — Absorption data for the remaining two fillers are somewhat simpler to describe, as no adjustement to the volume-fraction dependence is required. Figure 23 shows that the ab-sorption data for BKMB, normalized by volume fraction, is proportional to frequency raised to the power 0.55.

TBMB — Similarly, no adjustment to the volume fraction term is required to obtain con-sistent reduced absorption data for the case of TBMB filler. As shown in Fig. 24, however, the frequency dependence is unusual; at frequencies greater than 4 MHz there is no apparent change in absorption with increased frequency. A simple functional form that fits this data is $F^2/(2.5 + F^2)$. The lines drawn in this and the previous figures correspond to the equations given in Table 3.

MULTICOMPONENT MIXES — Both SGMB and BKMB were individually added to RTV-602 mixes containing 10 to 60 percent by weight FEOX. The loss measured is generally somewhat higher than that predicted from summing the terms in Table 3 for each component of the mix. This is not surprising. Clearly if there are appreciable multiple scattering losses in the single filler systems (as we suggest), the presence of an additional component will positively or negatively interfere with this cooperative loss. Closer agreement between data and predic-tion can be obtained by introducing the cross - terms listed in Table 3. It is noted, however, that the uncertainties present in these refinements are large, and the form of the equations used is largely intuitively assigned.

Fitting Equation Restrictions

The frequency interval of principle importance in the echo reduction calculations (presented in the following section) is 2.5 to 7.0 MHz. The fitting equations developed in this study reflect this. In constucting the fitting equations, we gave all data points equal (absolute) weight; since the attenuation values measured at high frequencies are generally much larger than those at low frequencies, the relative uncertainty associated with the higher frequency data

is therefore lower than that associated with the lower frequency measurements. This is consistent with the constraints imposed during the design of this experiment; namely, the apparatus dimensions and sample sizes chosen were selected to maximize the reliability of the absorption measurements over this same frequency range.

The terms in the absorption equation pertaining to the use of RTV-602, FEOX, SGMB, and perhaps also LGMB can probably be used at frequencies less than 2.5 MHz without introducing serious errors. However, the term pertaining to BKMB cannot; at frequencies below 2.5 MHz, its frequency dependence (0.55 power) is expected to be too gradual for reasonable estimates, and a transition to a squared frequency dependence is anticipated. The term corresponding to the addition of TBMB must be used with caution at all frequencies, since its frequency dependence is rather peculiar, and may be indicative of a multiple-scattering saturation condition.

Additionally, insofar as absorption is concerned, the batch-to-batch reproducibilty of these microballoons is not as good as we would wish. This became evident when we compared absorption data for a BKMB sample prepared from fresh microballoons with one prepared from microballoons recieved four years previously. In fact, the sample-to-sample reproducibility within this study is somewhat poorer than expected, although quite acceptable for present purposes. This could be due to small variations in the distribution characteristics of microballoon sizes, wall-thicknesses, or surface treatments, or in the case of BKMB and TBMB, to the absorption of water from the atmosphere. Regardless of the cause, the equations presented in Table 3 should be considered only as a guide or estimate of absorption when other microballoon batches are used.

ECHO REDUCTION ON FLAT PLATE

In this section, we show that the spraying procedure used does not noticeably alter the composition or bulk properties of the material deposited, and that coatings with predictable echo-reduction (ER) characteristics can be routinely applied. The spraying procedure itself is described in Appendix C.

The test performed is to compare measured ER values for thin coatings sprayed onto thick steel plates, with ER values predicted from theory using the previously measured bulk acoustic properties. If these experimental and theoretical ER values agree, then the intrinsic properties of the coating material are not significantly different from those of the corresponding bulk samples previously measured. This result would remove some concern that the use of these very high diluent concentrations and the atomization during spraying might alter either the filler concentrations in the deposited coating or the microscopic structural integrity of the coating material. A microphotograph of a typical spray-deposited coating is shown in Fig. 25.

Theoretical Description

The theoretical description we use is a simplification of the equations derived by Brekhovskikh [9], and previously tested by Barnard, Bardin, and Whiteley [10]. Our simplification is for normal incidence, so that shear terms may be neglected. For this case, the equations reduce to:

$$T = 2/\{(1 + Z_{31}) \cos (kd) + j(Z_{21} + Z_{32}) \sin (kd)\} \tag{12}$$

$$R = (T/2) \{(1 - Z_{31}) \cos (kd) + j(Z_{21} - Z_{32}) \sin (kd)\} \tag{13}$$

21

Fig. 25 — Microphotograph of a typical coating. Coating contains 3% SGMB and 30% FEOX, and is 0.033 cm thick (see Fig. 27).

where T and R are the pressure transmission and reflection coefficients respectively, and $Z_{mn} = Z_m/Z_n$. Sound is initiated in medium 3 (water), and interacts with media 2 and 1 (the coating and steel respectively). The parameters k and d are the wave number in the coating material ($k = 2$ pi F/C) and the thickness of the coating layer respectively. This wave number is complex, since the sound speed in the coating material is itself complex, C^*, and given by:

$$C^* = C/\sqrt{1 + (j/2979) \, (\alpha C/F)^2} \tag{14}$$

where F is the frequency, α is the attenuation in dB/cm, j is the square-root of -1, and C is the wave speed (the magnitude of the phase velocity). The factor 2979 can be eliminated if α is expressed in nepers, and angular frequency is used instead of frequency F. Since impedance is simply the product of sound speed and density, Z_2 is also complex; in this model, however, media 3 and 1 are considered lossless, and therefore Z_3 and Z_1 are not complex.

22

Echo reduction *ER* is then defined as:

$$ER = -20 \log R \tag{15}$$

and transmission loss *TL* is defined as:

$$TL = -20 \log (T Z_{13}) \tag{16}$$

where the factor Z_{13} must be included in this last equation to change from a pressure transmission coeficient to a more useful intensity-related one. Transmission loss is not used in the remainder of this report; Eq. 16 is included here only since *TL* must generally be considered in practical evaluations of the acoustic performance of coatings and layers.

Although these equations are useful, they do not present us with any physical explanation of the predicted *ER* or *TL* behavior. To better understand the *ER* behavior exhibited in our graphs, it is useful to first present a simple model which can account for most of the features observed. This model makes two assumptions: (a) the complex nature of impedance can be ignored, and (b) only the first two returned echos need be considered. The first of these assumptions is valid so long as the intrinsic absorption of the coating is small, while the second (described later in this section) is usually quite reasonable.

Using this simple model, we can then analyze the typical but hypothetical ER behavior depicted in Fig. 26. The reflected signal is composed of two components: signal 1 is a specular reflection from the water-coating interface, and signal 2, the specular reflection from the coating-steel interface. Since the second component travels farther than the first, these two components will generally be out of phase by the amount $2kd$. As frequency is increased, the measured ER will therefore exhibit oscillitory behavior, as the two signals alternately add and subtract. The amplitudes of these two signals can now be concidered. For the hypothetical case illustrated, signal 1 is 20 dB down from the incident signal, and (as usual) is independent of frequency. Signal 2, however, decreases with frequency since the intrinsic attenuation in the coating medium (as usual) increases with frequency. We can then bound these oscillitory ER values by two limits: one for the simple additon of the two signal amplitudes ignoring phase, and one for the corresponding simple subtraction. In Fig. 26 these are termed the phase-additive and phase-subtractive limits respectively. As frequency changes,a change is caused in the phase difference between these two components, the overall value of ER will oscillate between these two limits.

This simple model will allow us to gain some physical insight into the relative importance of these two components of the echo reductions presented in the remaining figures of this report. For example, if an ER graph appears to decrease with increasing frequency, and shows only small oscillation amplitudes, we can infer that we are in the low-frequency region and that most of the observed ER is being returned from the coating-steel interface; if there are large oscillation amplitudes, we conclude that the two signal amplitudes are comparable; likewise, if there are only small oscillation amplitudes, and no detectable monotonic decrease in signal amplitude with increasing frequency, we can infer that essentially all of the returned signal is coming from the water-coating interface.

This simple model cannot, of course, be carried too far. For example, it would follow from this simple model that large echo reductions can be achieved by simply mat ning the impedance of the coating to water, and using coating materials with very high intrinsic attenuation
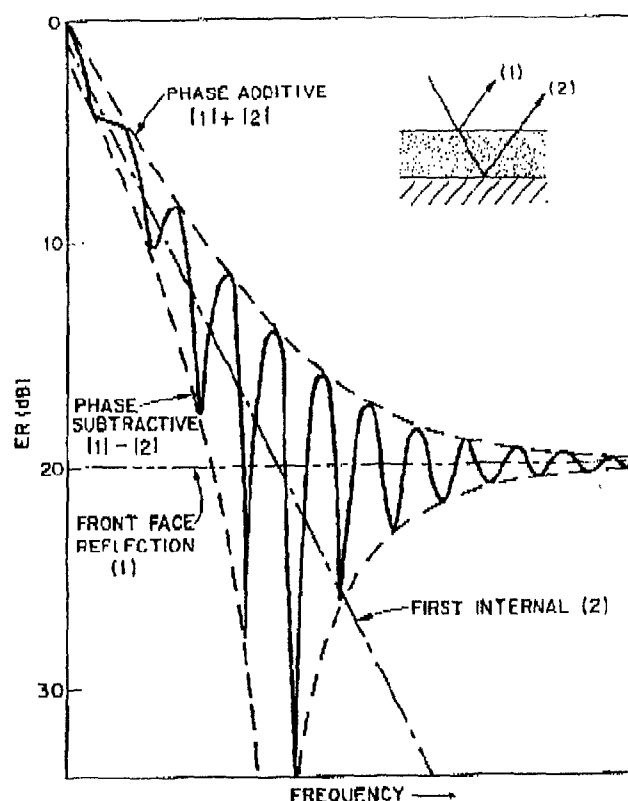
Fig. 26 — Simplified representation of ER response from a coated surface. Returned echo is considered as the sum of the specular reflections from the water-coating and the coating-steel interfaces.

values. Because this simple model does not include the complex nature of impedance, it does not recognize the contradiction in these two requirements. Nonetheless, this simple approach can be used as a guide in the development of coatings with specific ER or TL requirements, and as a tool for suggesting the relative importance of impedance matching and absorptive loss. For a more detailed discussion of sound interaction with ER coatings, the reader is referred to the book by Bobber [11].

Comparison of Experiment and Theory

Figures 27 through 32 show measured and predicted values of ER for various mixes. In these figures, the experimental data is shown by a continuous line, and the theoretical predictions are drawn as squares. The two curves are seen to be in agreement in all cases, particularly considering the experimental limitations involved.

The principal parameters used in this theory are density, wave speed, absorption, and coating thickness. Values for the first three of these were determined from the fitting equations presented in the previous sections. Thus, they were obtained from independent measurements on thick specimens, and used without adjustment in these calculations. The last of these, the
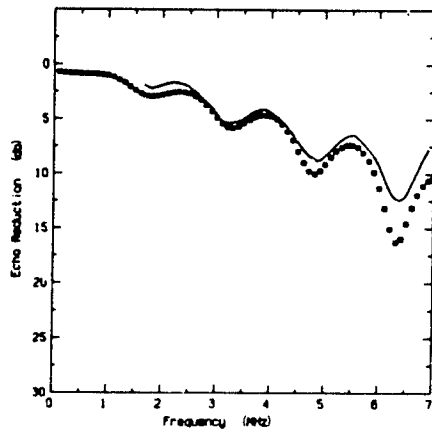
Fig. 27 — Measured (line) and predicted (squares) ER for coated steel plate. Coating contains 3% SGMB and 30% FEOX, and is 0.033 cm thick.
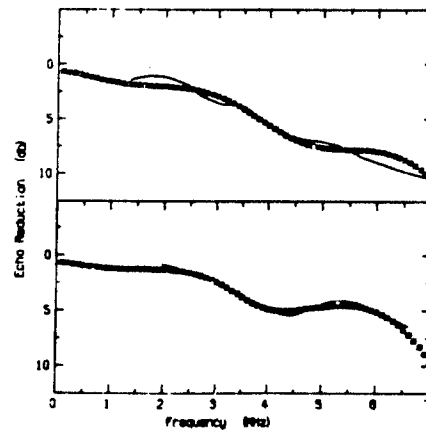

Fig. 28 — Measured (line) and predicted (squares) ER for coated steel plates. Upper and lower graphs correspond to coatings containing 5% SGMB, and respectively 50% FEOX (0.014 cm thick) and 30% FEOX (0.015 cm).
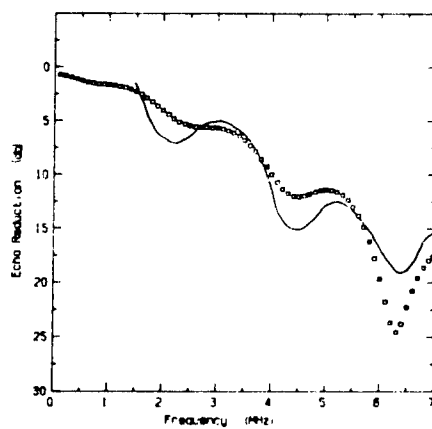

Fig. 29 — Measured (line) and predicted (squares) ER for coated steel plate. Coating contains 5% SGMB and 50% FEOX, and is 0.027 cm thick.
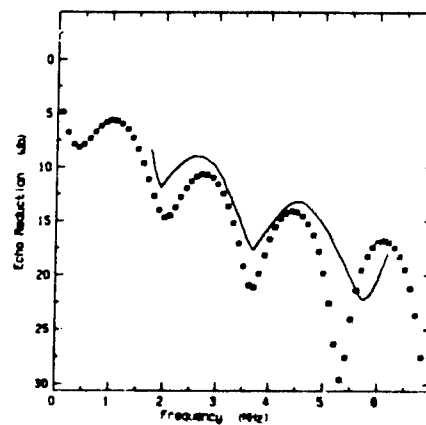

Fig. 30 — Measured (line) and predicted (squares) ER for coated steel plate. Coating contains 3% BKMB and 50% FEOX, and is 0.027 cm thick.
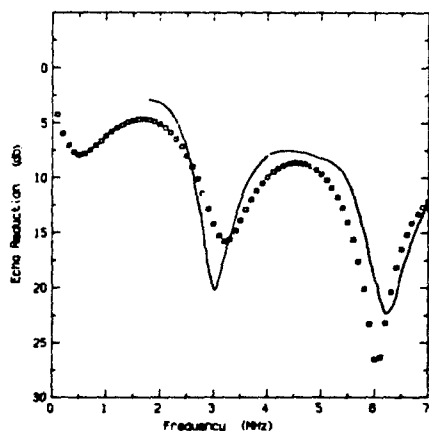
Fig. 31 — Measured (line) and predicted
(squares) ER for coated steel plate. Coating
contains 5% BKMB and 30% FEOX, and is
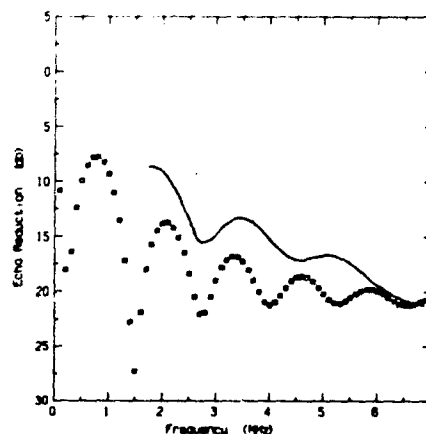0.077 cm thick.

Fig. 32 — Measured (line) and predicted
(squares) ER for coated steel plate. Coating
contains 5% BKMB and 50% FEOX, and is
0.037 cm thick.

coating thickness, proved difficult to measure accurately because of the compliance of the coating. Our initial thickness measurement technique involved using a long-arm dial indicator, a calibrated spacer block to cover the coating, and a flat surface plate. Only very light pressure was used. In a few cases these measurements were as much as 15% smaller than those made using a measuring microscope after the coating was stripped from the plate. Unfortunately, we did not recognize this problem until after the coatings had been removed from their backing plates. Rather than pursue this relatively unimportant point, we have used an average value of these two measurements, and allowed as much as 10% adjustment to this parameter when useful in obtaining better agreement between theory and experiment. This adjustment, however, is quite minor. It slightly alters the frequencies at which the minima and maxima occur, but is otherwise not noticeable.

Each of these figures are now considered separately. The first three are for coatings containing the low-loss SGMB fillers, while the last three are for higher-loss BKMB fillers.

Figure 27 shows the frequency dependence of ER for a relatively thick coating (0.033 cm); the frequency separation between adjacent maxima or minima is therefore small. The concentration of fillers is also relatively dilute (3% SGMB, 30% FEOX); consequently the intrinsic sound attenuation in the coating material is small, and most of the recieved echo is from reflection at the coating-steel interface. As frequency (and therefore intrinsic attenuation) is increased, the amplitude difference between maxima and minima increase, as predicted by our simple model. The agreement between prediction and experiment is seen to be very good in this figure.

Figure 28 shows the ER behavior of two thin coatings, nominally 0.014 cm thick, containing 5% SGMB, and also containing either 30% (bottom) or 50% (top) FEOX. The frequency separation between adjacent maxima or minima is seen to be large, as expected. Since the intrinsic attenuation in the coating is small, essentially all of the returned echo is again caused by reflection at the coating-steel interface. These two coatings, incidentally, are seen to have nearly flat frequency responses in the region 5 to 6 MHz.

26

Figure 29 shows the performance of a thicker (0.027 cm) coating of 5% SGMB and 50% FEOX. The oscillitory dependence of ER on frequency is apparent in this figure. The large echo reductions achieved indicate a good impedance match between the coating and water. Although the theoretical prediction and the experimental measurements are not in as good agreement as was evidenced in previous figures, the agreement is nonetheless satisfactory considering the experimental limitations involved.

Figure 30 shows the response of a coating containing 3% BKMB and 50% FEOX. As is apparent in Table 3, BKMB is a much more lossy filler than SGMB. Hence, the coating's intrinsic absorption is greater in these and the following figures than in the four previous ones. The behavior shown in Fig. 30 corresponds to the frequency region in which most of the returned echo comes from the coating-steel interface. As the frequency approaches 7 MHz, however, the magnitude of the ER minima indicate that the signals from the coating-water and coating-steel interfaces are becoming comparable.

Figure 31 corresponds to a thicker (0.077 cm) coating of 5% BKMB and 30% FEOX. The greater low-frequency intrinsic loss, and less rapid increase in this loss as frequency increases, cause large and persistent oscillations in the frequency dependence of echo reduction. Because this is a thick sample, these oscillations in ER are widely spaced in frequency.

Finally, Fig. 32 shows the ER response of a 0.037 cm thick coating containing 5% BKMB and 50% FEOX. The agreement between predicted and measured ER response is not as close as that found in the previous figures. This figure, as well as Fig. 29, is included principally to illustrate the deviations from predicted behavior that were encountered on occasion during the course of this study. As such, they are presented to provide the reader with some feeling for the degree of confidence that can be placed in the predicted ER response of coatings formulated and deposited using the methods and procedures described in this report.

It should be noted that these coating compositions were selected for interest in their detail, and are not optimized for any particular application. For example, the use of 53% FEOX would provide a better impedance match between the coating and water in most cases. In such cases, however, the small echo from the water-coating interface might not be measureable using the apparatus of this study. Similarly, coatings with greater intrinsic loss could have been used; however, in such cases the first echo dominates, and the graphs are unrevealing. Therefore, the coatings used here are more suitable for our application, i.e., verifying that the acoustic properties of the coating material are not degraded significantly by the spraying process.

CONCLUSIONS

We have constructed and acoustically characterized a materials system that fills the needs of our various acoustic studies. It consists of a rubber base, diluent, dense filler, and a selection of light microballoon fillers. By varying the concentrations of these fillers , the acoustic properties of the resulting rubber can be selected from a wide range of possible values. The diluent used (toluene) is ideal. It even can be added in large quantities (50% by volume), and yet, after its removal from the mix (either before or after the rubber cures), the measured acoustic properties of the resulting rubber are in close agreement with those obtained for comparable mixtures not containing toluene.

These rubbers have been used to form molded articles with well-defined bulk acoustic properties, or using the spraying procedure described in this report, they have been deposited as thin coatings. Measured values of the echo-reduction characteristics of these coatings are in good agreement with theoretical predictions based on the established bulk properties of materials deposited; this indicates that the acoustic properties of the coating material are not significantly altered by the spray-deposition process.

In summary, the materials system described here fills our needs, and is expected to find considerable use in our future investigations.

REFERENCES

1. R. H. Vogt, L. Flax, L. R. Dragonette, and W. G. Neubauer, J. Acoust. Soc. Am., **57**, 558 (1975)

2. L. Flax and W. G. Neubauer, ibid **61**, 307 (1977)

3. L. S. Schuetz and W. G. Neubauer, ibid **62**, 513 (1977)

4. J. D. Ryder, P. H. Rogers, and J. Jarzynski, ibid **59**, 1077 (1976)

5. R. D. Corsaro and J. Jarzynski, submitted to J. Acoust. Soc. Am.

6. R. C. Weast, editor, *CRC Handbook of Chemistry and Physics*, 58th edition, page B-121, CRC Press Inc., Cleveland, Ohio (1977-78).

7. Z. Haskin, in *Mechanics of Composit Materials*, editors F. W. Wendt, H. Liebowitz and N. Perrone, Pergamon Press, N. Y. (1967)

8. J. R. Allegra and S. A. Hawley, J. Acoust. Soc. Am. **51**, 1545 (1972)

9. L. M. Brekhovskikh, *Waves in Layered Media*, Academic Press, N. Y. (1960)

10. G. R. Barnard, J. L. Bardin, and J. W. Whiteley, J. Acoust. Soc. Am. **57**, 577 (1975)

11. R. J. Bobber, *Underwater Electroacoustic Measurements*, U. S. Government Printing Office, Washington, D. C. (1975)

Appendix A
SYMBOLS

SUBSCRIPTS

b	value for BKMB
i	values for the pure state of the i-th component
l	value for LGMB
m	properties of the mix formed
o	initial or reference value
r	reference level
s	value for SGMB
t	value for TBMB
w	value for water
x	value for sample
1,2,3	values for media 1(in which sound is initiated), 2 (sample or coating), and 3 (backing)

LABELS

Σ	summation over all components
log	base 10 logarithm
α	attenuation (dB/cm unless noted otherwise)
A	proportionality constant
C	longitudinal wave speed
C^*	complex longitudinal wave speed
d	sample thickness
F	frequency (MHz unless noted otherwise)
J	$\sqrt{-1}$
K	bulk modulus
K^*	calculated value of K for composite-sphere model
k	wave number
κ	compressibility
P	sound pressure level
R	reflection coefficient
ρ	density
S	shear modulus
t	time of flight
T	transmission coefficient
w, v	actual weights and volumes
W, V	weight and volume fractions
Z	impedance

29

Appendix B
IDEAL MIXTURE MODEL

As usual, weight fraction is defined as:

$$W_i = w_i/w_m \qquad (B1)$$

hence:

$$\Sigma \, W_i = 1 \qquad (B2)$$

The one assumption of the ideal mixture model (also called the simple rule of mixtures) is that the volumes of the components are additive; that is, there is no expansion or shrinkage on mixing. Thus:

$$v_m = \Sigma \, v_i \qquad (B3)$$

Hence the usual definition of volume fraction:

$$V_i = v_i/v_m \qquad (B4)$$

where

$$\Sigma \, V_i = 1 \qquad (B5)$$

takes on a somewhat different interpretation; the volume v_i is now simply the actual volume of the i-th component added, rather then an indirect quantity representing a partial volume of the material as inferred from the measured volume change for the addition of each component.

This assumption is usually not valid if there is substantial mixing on the molecular level, as is generally the case with liquids or solutions. On the other hand, it is quite reasonable for describing aggregates, such as the filled rubbers used in this study.

Using this assumption, one can then readily derive an expression for the density of the final mix, in terms of the densities and volume fractions of the components used:

$$\rho_m = w_m/v_m$$
$$= \Sigma \, [w_i/v_m]$$
$$= \Sigma \, [\rho_i v_i/v_m]$$
$$\rho_m = \Sigma[\rho_i V_i] \qquad (B6)$$

Similarly, compressibility can be expressed in terms of the compressibilities and volume fractions of the pure components:

30

$$\kappa_m = (1/v_m) \ d/dP[v_m]$$
$$= (1/v_m) \ d/dP[\Sigma \ v_i]$$
$$= \Sigma \ [(1/v_m) \ d/dP(V_i)]$$
$$\kappa_m = \Sigma \ V_i \ \kappa_i \tag{B7}$$

where the pressure derivative d/dP is taken at constant temperature.

Since mixtures are generally prepared by weight, rather than by volume, it is useful to express these quantities in terms of weight fractions. Volume fraction is then:

$$V_i = [w_i/\rho_i]/[w_m/\rho_m]$$

or:

$$V_i = W_i \ \rho_m/\rho_i \tag{B8}$$

and density is found to be:

$$1/\rho_m = [w_i/\rho_i]/w_m$$

or:

$$1/\rho_m = [W_i/\rho_i] \tag{B9}$$

Compressibility is best calculated from weight fraction by first using Eq. B8 to determine volume fraction, and then substituting this into Eq. B7.

Appendix C
SPRAYING PROCEDURE FOR COATING APPLICATION

The coating was applied using a commercial-type paint sprayer with pressurized feed (Simco-Bendix Model 9 Spray Gun). In this study the coating was applied only to a flat steel plate, which was 1.90 cm (3/4 in) thick, however the procedure described here also has been successfully used to deposit coatings on objects with more complicated shapes.

The mix to be sprayed is first diluted with nominally one milliliter of toluene per gram of mix, to obtain the low viscosities necessary for uniform spray deposition. The SRC-05 catalyst is then added at the concentration 1.1% by weight of resin (RTV-602).

The coating is deposited using a regulated air pressure of 170 kPa (25 psi), with the gun's air vent closed as much as possible. A number 4 needle, nozzle, and airhead is used, and a round spray pattern is selected. The setting of the atomizer is approximately 1 to 1 1/4 turns out from the closed position, and the needle valve setting is approximately 1 1/4 to 1 1/2 turns out from closed. The plates were positioned vertically, and sprayed in a horizontal pattern, with each pass being approximately 2.5 cm lower than the previous one until the entire plate is covered. This constitutes one coat approximately 25 μm (1 mil) thick. After each coat, the plate is rotated 90 degrees for better uniformity, and, after a pause of seven seconds, the next coat is applied. During the pause, the spray gun is shaken by hand, to assure a uniform mix of the coating material.

When properly sprayed, the coating has a grainy appearance immediately after deposition, but quickly levels to form a smooth surface with no obvious grain. During operation, the appearance can be described as wet, but after the seven r   between coats it is only slightly damp. If the coating is applied at too i   osited too thickly during a single pass, the surface takes on an orange   greatly overdone, the coating runs. Equally detrimental, if the coating   ally or too slowly, a loose, pebbly, low-gloss surface results. This is due either   drying of the mix in the air stream before deposition takes place, or to the   ing   the previous coat which can cause poor adhesion between coats.

On occasion the nozzle becomes partially clogged, but it can usually be blown clear using several short bursts from the gun. Nozzle clogging is most likely to become a problem when the deposition rate is too slow, or the gun has been inactive for more than ten seconds. After a period of inactivity, the needle valve adjusting screw should be backed out 1/2 turn, and the mixture sprayed for several seconds while slowly returning to the original setting; this procedure helps clear the nozzle of any buildup.

For safety, all spraying should be done in a well ventilated fume hood, because quite large amounts of toluene are vaporized during this spraying operation. As with any paint spraying, a substantial amount of time should be allocated for clean-up.